



Inhibition of the ATR kinase enhances 5-FU sensitivity independently of nonhomologous end-joining and homologous recombination repair pathways

Received for publication, April 19, 2020, and in revised form, July 13, 2020. Published, Papers in Press, July 16, 2020, DOI 10.1074/jbc.RA120.013726

Soichiro S. Ito^{1,†}, Yosuke Nakagawa^{1,‡}, Masaya Matsubayashi², Yoshihiko M. Sakaguchi², Shinko Kobashigawa², Takeshi K. Matsui^{2,3}, Hitoki Nanaura^{2,3}, Mari Nakanishi², Fumika Kitayoshi², Sotaro Kikuchi², Atsuhisa Kajihara¹, Shigehiro Tamaki¹, Kazuma Sugie³, Genro Kashino⁴, Akihisa Takahashi⁵, Masatoshi Hasegawa⁶, Eiichiro Mori^{2,*}, and Tadaaki Kiritani^{1,*}

From the Departments of ¹Oral and Maxillofacial Surgery, ²Future Basic Medicine, ³Neurology, and ⁶Radiation Oncology and the ⁴Radioisotope Research Center, Nara Medical University, Kashihara, Nara, Japan and the ⁵Gunma University Heavy Ion Medical Center, Maebashi, Gunma, Japan

Edited by Patrick Sung

The anticancer agent 5-fluorouracil (5-FU) is cytotoxic and often used to treat various cancers. 5-FU is thought to inhibit the enzyme thymidylate synthase, which plays a role in nucleotide synthesis and has been found to induce single- and double-strand DNA breaks. ATR Ser/Thr kinase (ATR) is a principal kinase in the DNA damage response and is activated in response to UV- and chemotherapeutic drug-induced DNA replication stress, but its role in cellular responses to 5-FU is unclear. In this study, we examined the effect of ATR inhibition on 5-FU sensitivity of mammalian cells. Using immunoblotting, we found that 5-FU treatment dose-dependently induced the phosphorylation of ATR at the autophosphorylation site Thr-1989 and thereby activated its kinase. Administration of 5-FU with a specific ATR inhibitor remarkably decreased cell survival, compared with 5-FU treatment combined with other major DNA repair kinase inhibitors. Of note, the ATR inhibition enhanced induction of DNA double-strand breaks and apoptosis in 5-FU-treated cells. Using gene expression analysis, we found that 5-FU induced the activation of the intra-S cell-cycle checkpoint. Cells lacking *BRCA2* were sensitive to 5-FU in the presence of ATR inhibitor. Moreover, ATR inhibition enhanced the efficacy of the 5-FU treatment, independently of the nonhomologous end-joining and homologous recombination repair pathways. These findings suggest that ATR could be a potential therapeutic target in 5-FU-based chemotherapy.

One of many anticancer agents available, 5-fluorouracil (5-FU) has nonetheless become the drug of choice in the treatment of various solid tumors because of its properties. It converts to a number of active metabolites (such as fluorouridine triphosphate, fluorodeoxyuridine triphosphate (FdUTP), and fluorodeoxyuridine monophosphate (FdUMP)) that disrupt RNA and DNA metabolism and inhibit thymidylate synthase (TS) (1, 2). Specifically, global RNA metabolism is compromised when the following conditions take place: 1) RNA absorbs the 5-FU-converted active metabolite, fluorouridine

triphosphate, in place of UTP, and 2) FdUTP, instead of dTTP, is absorbed by DNA (2, 3). A third process occurs and results in DNA damage. The absorption of FdUMP contributes to an inhibition of TS via the formation of a ternary covalent complex that consists of TS-FdUMP-5,10-methylenetetrahydrofolate. It also blocks cells from the synthesis of dTMP from dUMP, causing cellular dUTP increases at the expense of dTTP. This leads to a significant misincorporation of dUTP or FdUTP during replication and, in particular, that of DNA.

Despite consistent observations of DNA damage as one of the 5-FU-mediated tumor cell killings (4, 5), the exact mechanism behind the processing and contribution of misincorporated dUTP and FdUTP to cytotoxicity has yet to be fully elucidated. Studies suggest that base excision repair (BER) enzymes and mismatch repair (MMR) identify misincorporated FdUTP and dUTP for excision from DNA (5–7). The BER enzyme uracil-DNA-glycosylase initiates repair of DNA through the elimination of uracil or 5-FU from DNA (8). However, this repair mechanism is rendered ineffective, given high FdUTP/dTTP ratios, and only serves to trigger the incorporation of additional false nucleotides (4). The MMR system plays an equally significant role in the correction of such replication errors via the nicks and gaps in single-strand DNA (ssDNA) produced by the FdUTP and dUTP in both BER and MMR (4). These nicks and gaps trigger the initial activation of ATR-checkpoint kinase 1 (Chk1) pathways, and activated Chk1 molecules, in turn, stop DNA replication. During these processes, unstable conformations in the DNA structure are induced by the coating of stalled replication fork complexes with replication protein A. The presence of excessive single-strand breaks (SSBs) at stalled replication forks subsequently induces DNA double-strand breaks (DSBs) in 5-FU-treated cells (9, 10).

DNA damage response (DDR) involves the activation of a signaling network that provides time for DNA repair and triggers apoptosis when extensive damage occurs. It effectively mediates cell-cycle arrest and is triggered by the activation of protein kinases, ataxia telangiectasia mutated (ATM), ATM and Rad3-related (ATR), and DNA-dependent protein kinase catalytic subunit (DNA-PKcs), which is one of three members of the phosphoinositide-3-kinase-like protein kinase (PIKK)

This article contains supporting information.

[†]These authors contributed equally to this work.

* For correspondence: Eiichiro Mori, emori@naramed-u.ac.jp; Tadaaki Kiritani, tkiritani@naramed-u.ac.jp.

This is an Open Access article under the [CC BY](https://creativecommons.org/licenses/by/4.0/) license.

family. Cell-cycle progression in G₁, S, or G₂ phase is delayed as these kinases recruit repair machinery to damaged DNA sites via the activation of effector checkpoints (11). Through p21/CIP1/WAF1 up-regulation, p53 mediates G₁ arrest and, where extensive DNA damage is detected, triggers apoptosis (12). Nonetheless, as a majority of cancer cells display loss of p53 function and its regulatory pathways, it is evident that chemotherapy-induced DNA damage is unable to halt G₁ phase or promote apoptosis. Cells rely solely upon S and G₂/M checkpoints for the arrest of the cell cycle and facilitation of DNA repair after genotoxic exposure and prior to mitosis. ATR/Chk1 kinases have been found to be implicated in the regulation of post-genotoxic stress cell-cycle arrest, impediment of subsequent replication origin firing during S phase, and involvement in the intra-S and G₂/M checkpoints (13–16).

Homologous recombination (HR) repair is one of the major DSB repair pathways (17, 18) that operates primarily via intact sister chromatids during late S and G₂ phases, but not at G₁ phase (19, 20). BRCA2, Rad52, Rad54, and Rad51 paralogs such as Rad51C-XRCC3 and Rad51B-Rad51C-Rad51D-XRCC2 are some of the proteins involved in vertebrate cells HR (21). BRCA2, an upstream protein, has been shown to regulate Rad51 activity (22). Mutations in the BRCA2 gene have consistently been found in hereditary breast (23) and ovarian cancers (24).

We previously demonstrated that BRCA2, a major component of the HR repair pathway, plays a crucial role in protecting cells from cell death and in the repair of DNA damage induced by 5-FU (3). However, the manner in which cells detect and respond to DNA damage induced by 5-FU remains unclear. ATR is activated in response to replication stress induced by DNA-damaging reagents and acts upon the upstream of BRCA2-dependent repair pathway (25–28). ATR is one of the principal kinases of the DNA damage response, in addition to ATM and DNA-PK. In the present study, we sought to characterize the role of ATR in response to 5-FU and examine the effect of an ATR inhibitor for cancer treatment with 5-FU.

Results

ATR inhibition sensitized 5-FU-treated cells

To examine the activation of ATR and other major DDR kinases by 5-FU treatment, we verified the phosphorylation of ATR, ATM, DNA-PKcs, and Chk1 by Western blotting in SAS cells. The phosphorylation of ATR at Thr-1989 (an autophosphorylation site) (29) was induced by 5-FU in a dose-dependent manner (Fig. 1), suggesting that 5-FU treatment activated ATR. Chk1 phosphorylation at Ser-345, a substrate of ATR/ATM kinase, induced by 5-FU was also detected in a dose-dependent manner, similar to the induction of ATR phosphorylation (Fig. 1), suggesting that Chk1 phosphorylation at Ser-345 by 5-FU is ATR-dependent. On the other hand, the phosphorylation of ATM at Ser-1981 induced by 5-FU was confirmed sufficiently even at 10 μ M, and more phosphorylation of DNA-PKcs at Ser-2056 induced by X-ray (20-gray) irradiation was detected than that induced by 5-FU (Fig. 1). These results suggest that 5-FU induces DNA damage to activate DDR signaling independent of simple DSBs, such as ionizing radiation-induced DSBs.

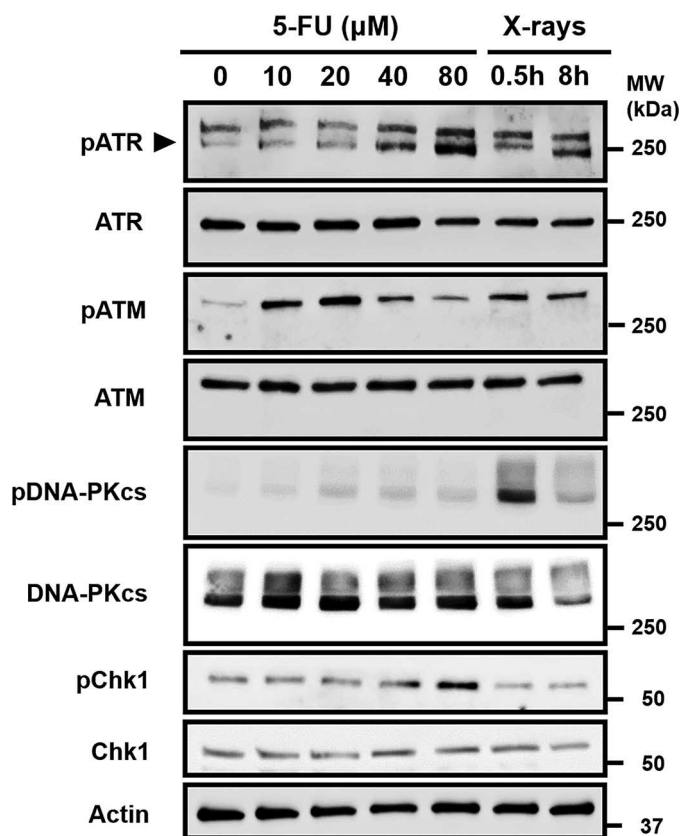


Figure 1. Phosphorylation of three members of the PIKK family and Chk1. Phosphorylation of ATR, ATM, DNA-PKcs, and Chk1 by 5-FU treatment for 24 h in SAS cells is shown. Cells were collected immediately after treatment. Irradiated cells were collected at 0.5 and 8 h after X-ray irradiation (20 Gy). Arrow, phosphorylated form of ATR. The top bands are nonspecific. All experiments were replicated three times.

To check whether the concentration of a specific inhibitor against ATR (ATRi) alone does not exceed IC₅₀ in our experiments, we analyzed cell survival. The surviving fraction showed a slight decrease under 10 μ M ATRi (Fig. S1, A and B), and the IC₅₀ value was \sim 15 μ M in Chinese hamster lung fibroblasts (Fig. S1A) and 5 μ M in SAS cells (Fig. S1B). Although 3 μ M ATRi alone did not have cell lethality, it synergistically enhanced the cytotoxicity of 5-FU treatment (Fig. 2A).

To verify the significance of ATRi compared with other major DDR kinase inhibitors against DNA-PK (DNA-PKi) and ATM (ATMi), SAS and HSC3 cells were exposed to 5 μ M 5-FU and 3 μ M ATRi/DNA-PKi/ATMi for 24 h and subsequently measured using a standard colony-forming assay. The number of surviving fractions was significantly lower in 5-FU treatment combined with ATRi, compared with 5-FU treatment combined with DNA-PKi or ATMi (Fig. 2A). We confirmed cell viability using a standard colony-forming assay by changing the concentration of 5-FU. The surviving fraction was remarkably decreased in the 5-FU treatment combined with ATRi compared with 5-FU alone in both SAS and HSC3 cells (Fig. 2B). The number of surviving fractions was lower in 5-FU treatment combined with ATRi, compared with 5-FU treatment combined with DNA-PKi or ATMi (Fig. 2, C and D). The surviving fraction decreases in 5-FU combined with ATRi are assumed to occur in a p53-independent manner (Fig. S1C). These findings

Inhibition of the ATR kinase enhances 5-FU sensitivity

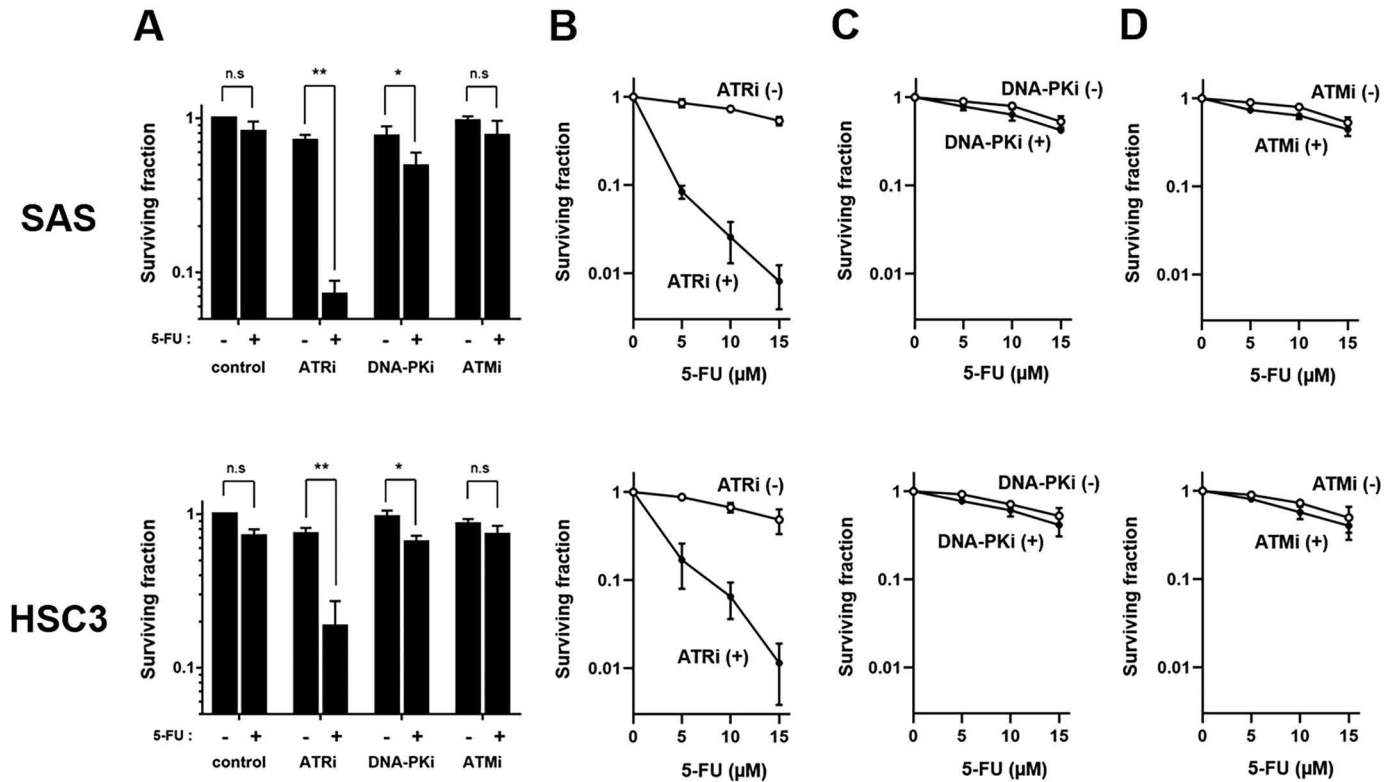


Figure 2. Sensitivity of three members of the PIKK family inhibition against 5-FU-treated SAS cells and HSC3 cells. A, ATRi, DNA-PKi, and ATMi were used at 3 μM , respectively. 5-FU was used at 5 μM . The surviving fraction was significantly decreased in 5-FU treatment combined with ATRi compared with treatments combined with either DNA-PKi or ATMi. B–D, surviving fraction in 5-FU-only treatment (open circles) was compared against 5-FU treatment combined with 3 μM ATRi (B)/DNA-PKi (C)/ATMi (D) (filled circles) in SAS (top column) and HSC3 (bottom column). All experiments were replicated three times. The values obtained are shown as means \pm S.D. (error bars). Data were compared statistically using the two-tailed Student's *t* test. * and **, $p < 0.05$ and $p < 0.01$, respectively. n.s., not significant.

suggest that ATRi is more effective in 5-FU treatment than DNA-PKi or ATMi. Fig. 3 (A and B) demonstrates that ATRi suppressed the phosphorylation of ATR and Chk1 induced by 5-FU, suggesting that ATRi blocks both ATR autophosphorylation and Chk1 phosphorylation.

ATR inhibition enhanced induction of DSBs in 5-FU-treated cells

To confirm the degree of DSB induction, we performed comet assays under neutral conditions. SAS cells were treated with 10 μM 5-FU and/or 3 μM ATRi for 12 h. The tail moments by 5-FU alone and 5-FU combined with ATRi were $10.3 \pm 2.5\%$ and $48.1 \pm 12.8\%$, respectively (Fig. 4 (A and B) and Fig. S2). The tail moments of 5-FU treatment combined with ATRi were significantly increased (Fig. 4B). These results suggest that ATR inhibition enhances DSB accumulation in cells treated with 5-FU.

In addition, we performed another method for detecting DSBs. γH2AX immunocytochemical staining is a sensitive method by which DSBs can be detected (30). This was used to examine the presence of H2AX phosphorylation induced by 5-FU and ATRi. Fig. 5A depicts a typical H2AX phosphorylation in SAS cells after 12-h treatment with 10 μM 5-FU and/or 3 μM ATRi. The percentages of H2AX phosphorylation (≥ 25 foci/cell)-positive cells treated with ATRi alone, 5-FU alone, and 5-FU combined with ATRi were 0.7 ± 0.5 , 45.2 ± 12.5 , and $78.4 \pm 3.6\%$, respectively, whereas the percentages of pan-nuclear

H2AX phosphorylation-positive cells treated with ATRi alone, 5-FU alone, and 5-FU combined with ATRi were 0.0 ± 0.0 , 4.7 ± 1.5 , and $35.5 \pm 4.0\%$, respectively (Fig. 5B). A significant increase in γH2AX foci or pan-nuclear γH2AX was observed in cells treated with 5-FU combined with ATRi (Fig. 5C). These results suggest that ATR inhibition enhances γH2AX foci formation in cells treated with 5-FU.

To quantify the optical intensity of H2AX phosphorylation using flow cytometry, cells were exposed to 10 μM 5-FU with or without 3 μM ATRi for 6 and 12 h (Fig. 6A). The intensity of H2AX phosphorylation treated with 5-FU alone for 6 h was 103.7 ± 0.6 , and for 12 h it was 119.1 ± 0.7 , whereas the intensity after a 5-FU combined with ATRi treatment for 6 h was 105.4 ± 0.3 , and for 12 h it was 162.1 ± 1.8 in SAS cells (Fig. 6B). The intensity of H2AX phosphorylation treated with 5-FU alone for 6 h was 110.6 ± 0.8 , and for 12 h it was 237.9 ± 2.3 , and after 5-FU combined with ATRi treatment for 6 h, it was 118.7 ± 0.6 , and for 12 h it was 364.3 ± 3.8 in HSC3 cells (Fig. 6B). Our findings suggest that ATR inhibition leads to a less efficient repair of 5-FU-induced DNA damage. These results suggest that ATR inhibition enhances H2AX phosphorylation in cells treated with 5-FU.

ATR inhibition enhanced apoptosis induced by 5-FU

To assess the apoptosis induction, cells were detected and quantified with a Hoechst33342 staining assay (Fig. 7A). The

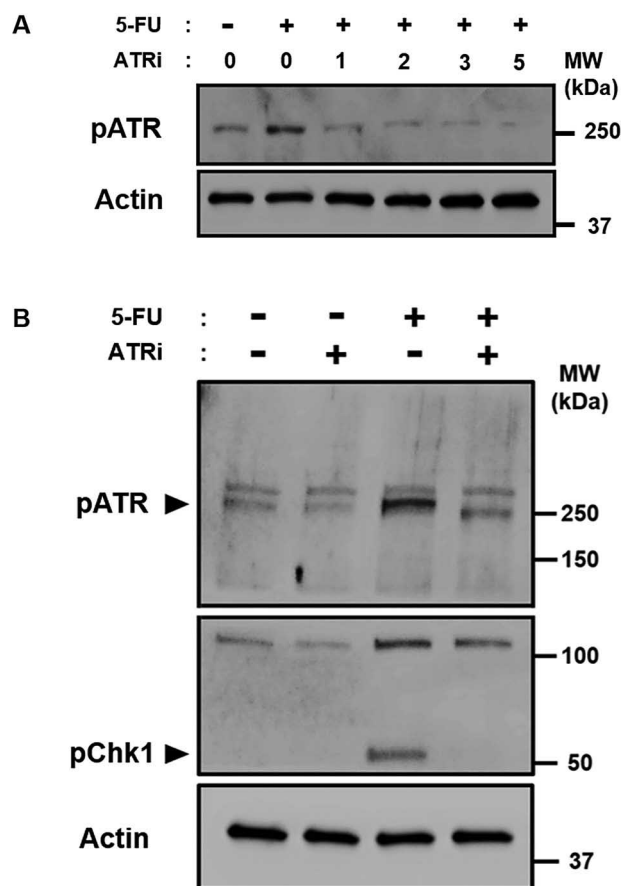


Figure 3. The phosphorylation of ATR and Chk1 induced by 5-FU treatment was suppressed by ATR inhibitor VE-821. *A*, expression analysis by Western blotting of ATR in SAS cells. ATRi was used at 1, 2, 3, and 5 μM . 5-FU was used at 10 μM . Cells were simultaneously treated by both chemicals for 24 h. *B*, expression analysis by Western blotting of ATR and Chk1. ATRi was used at 3 μM . 5-FU was used at 10 μM . Cells were simultaneously treated by both chemicals for 24 h. Cells were collected immediately after treatment. ATR and its major downstream effector, Chk1, were phosphorylated by 5-FU treatment. In addition, these phosphorylations were suppressed by ATRi. Arrow, phosphorylated form of ATR and Chk1. Top bands are nonspecific. All experiments were replicated three times.

fraction of apoptosis by 3 μM ATRi alone, 10 μM 5-FU alone, and 10 μM 5-FU combined with 3 μM ATRi for 12 h was 12.9 ± 5.3 , 15.6 ± 6.9 , and $40.5 \pm 5.1\%$, respectively, and 11.3 ± 2.0 , 30.6 ± 5.8 , and $59.8 \pm 15.5\%$, respectively, for 24 h in SAS cells (Fig. 7B). Counterparts for 12 h were 8.6 ± 3.8 , 15.5 ± 8.5 , and $30.0 \pm 16.6\%$ respectively, and 15.6 ± 6.9 , 46.0 ± 11.0 , and $66.4 \pm 11.5\%$, respectively, for 24 h in HSC3 cells (Fig. 7B). Apoptotic bodies appeared at a higher frequency in cells given 5-FU treatment combined with ATRi both in SAS and HSC3 cells (Fig. 7, A and B). These results suggest that ATR inhibition enhances apoptosis induction in cells treated with 5-FU.

To analyze the cell-cycle profile after 5-FU treatment, we examined the cell-cycle distribution. When DNA fragmentation occurred, the position of apoptotic cells was shifted to lower DNA content values, and a sub- G_1 population was detected far to the left of the G_1 peak (31, 32). Cells were exposed to 10 μM 5-FU and/or 3 μM ATRi for 8, 16, and 24 h (Fig. 8A). After treatment with 5-FU alone for 8, 16, and 24 h, the fraction of sub- G_1 was 3.3 ± 0.3 , 14.8 ± 0.2 , and $38.1 \pm 2.8\%$, and after treatment with 5-FU and ATRi for 8, 16, and 24

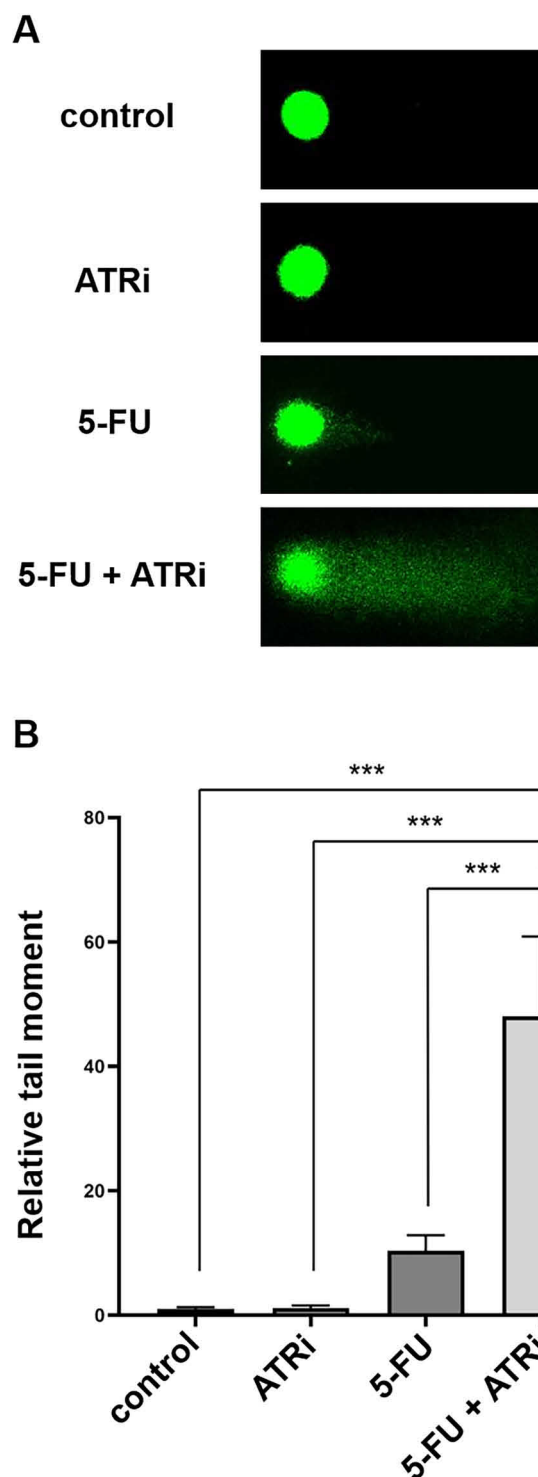


Figure 4. DSBs analysis by neutral comet assay. *A*, typical images of comet assays in SAS cells. Cells were exposed to 10 μM 5-FU and/or 3 μM ATRi treatment for 12 h. *B*, the tail moments of more than 50 cells were quantified. All experiments were replicated three times. The values obtained are indicated as means \pm S.D. (error bars). Data were compared statistically using the two-tailed Student's *t* test: ***, $p < 0.001$.

h, it was 8.8 ± 0.1 , 49.6 ± 3.8 , and $68.1 \pm 1.0\%$ in SAS cells (Fig. 8B). The counterparts were 4.3 ± 0.1 , 12.2 ± 0.2 , and $15.1 \pm 0.3\%$ and 18.8 ± 0.6 , 46.0 ± 1.7 , and $68.2 \pm 1.4\%$ in HSC3 cells (Fig. 8B). The fraction of sub- G_1 was remarkably increased in 5-FU treatment combined with ATRi compared with 5-FU

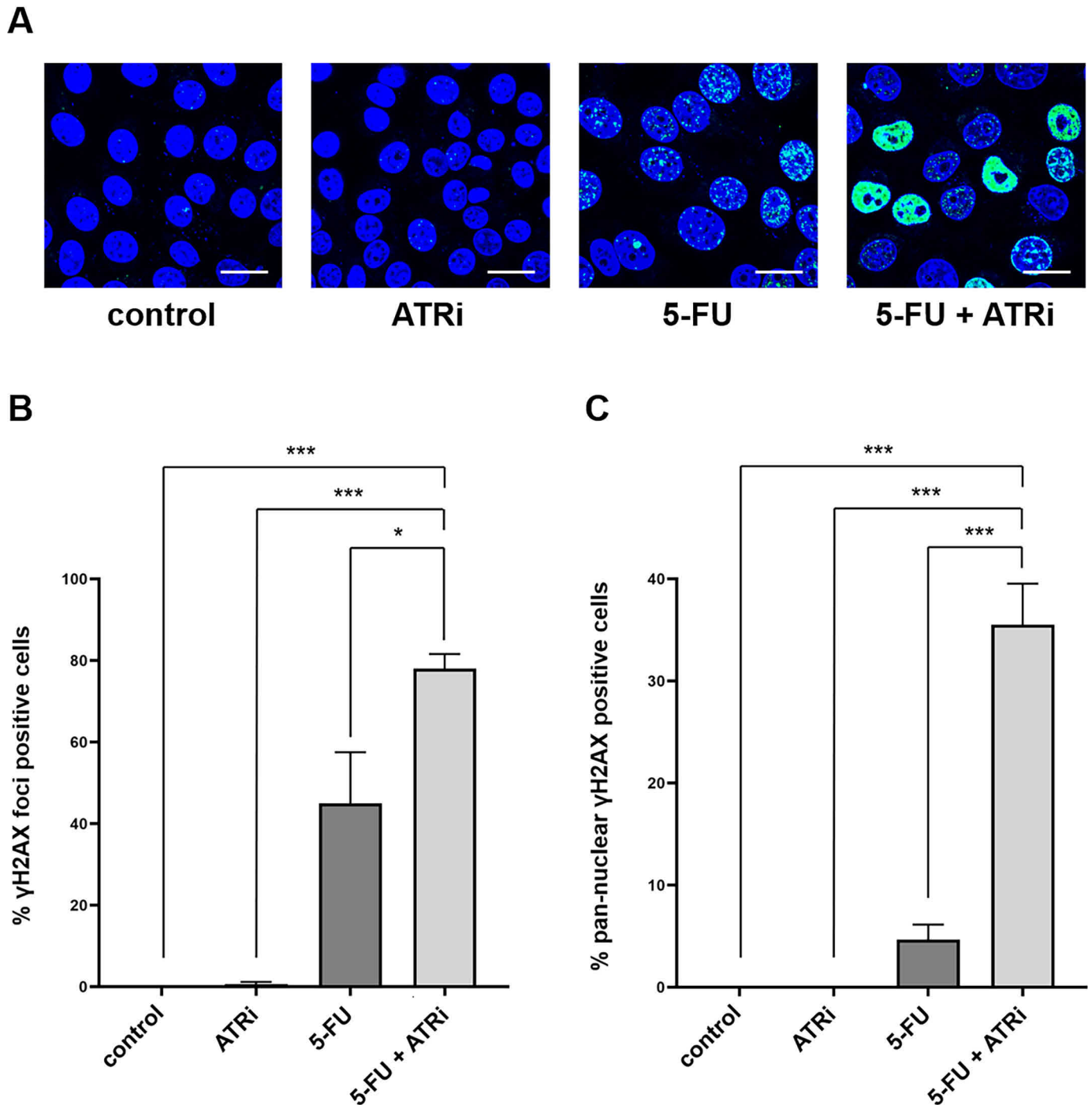


Figure 5. Histone H2AX phosphorylation analysis by immunostaining. *A*, phosphorylation of histone H2AX was detected in SAS cells. Cells were exposed to 10 μM 5-FU and/or 3 μM ATRi treatment for 12 h. *B*, quantitative data of histone H2AX phosphorylation (≥ 25 foci/cell)-positive cells. *C*, quantitative data of pan-nuclear histone H2AX phosphorylation-positive cells. Bars, 20 μm . All experiments were replicated three times. The values obtained are indicated as means \pm S.D. (error bars). Data were compared statistically using the two-tailed Student's *t* test: * and ***, $p < 0.05$ and $p < 0.001$, respectively.

treatment alone. These results suggest that ATR inhibition enhances fragmentation of cellular nucleus in cells treated with 5-FU.

5-Fu induced cell-cycle arrest between S phase and mitotic phase

Based on the cell-cycle analysis, 5-FU treatment caused cell-cycle arrest in S phase at 8 and 16 h (Fig. 8A). To investigate the

nature of the cell-cycle arrest involved in the response to 5-FU treatment, we analyzed genome-wide mRNA by bulk RNA-Seq. The 32 genes that regulated significantly were detected by differentially expressed gene analysis both in SAS and HSC3 (Fig. 9 (A and B), Fig. S3 (A–C), and Table S1). We then screened nine genes associated with the cell cycle from the 32 genes by gene ontology (GO) analysis. The expression of four genes, cyclin E1 (*CCNE1*), cyclin E2 (*CCNE2*), cyclin-dependent

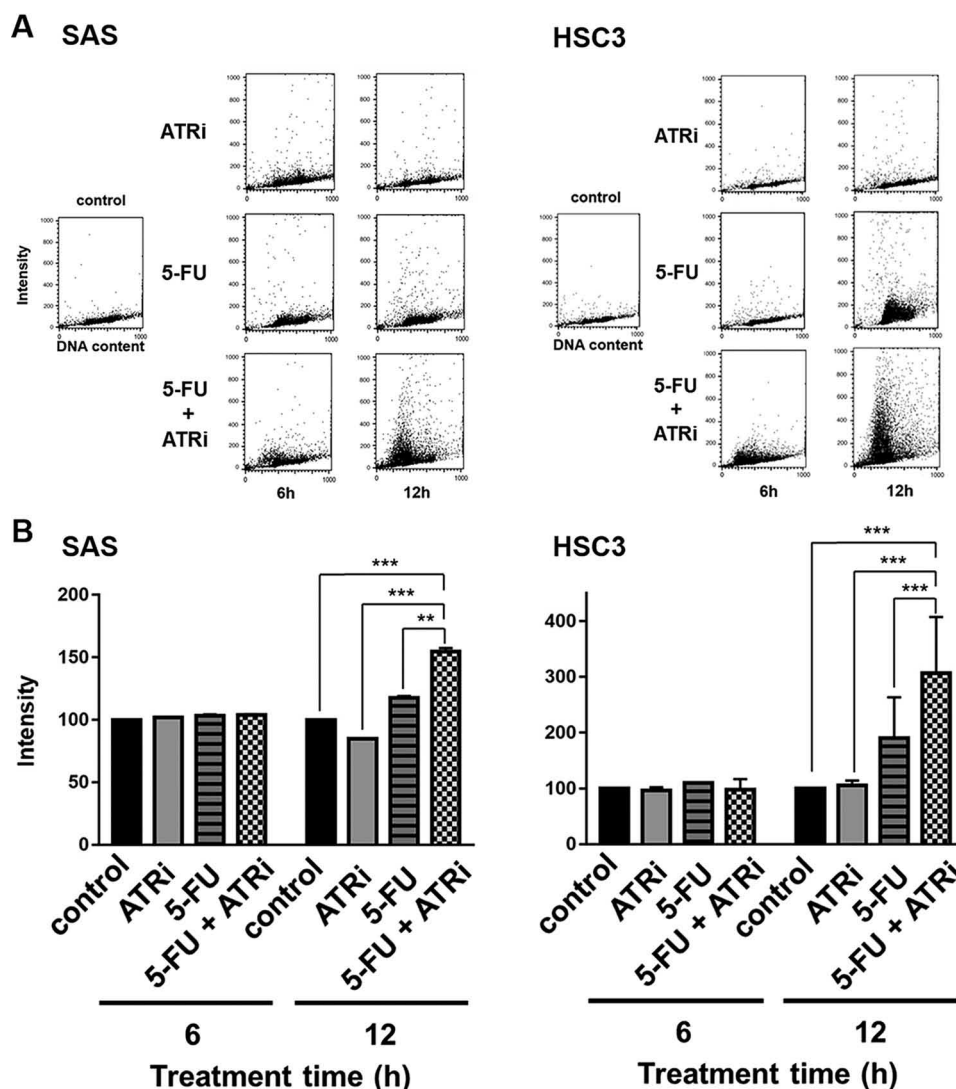


Figure 6. Histone H2AX phosphorylation analysis by flow cytometry. A, phosphorylation of histone H2AX was measured using flow cytometry in SAS cells and HSC3 cells. Cells were exposed to 10 μM 5-FU and/or 3 μM ATRi treatment for 6 and 12 h. B, phosphorylation intensity was schematized as illustrated in SAS and HSC3. All experiments were replicated three times. The values obtained are indicated as means \pm S.D. (error bars). Data were compared statistically using the two-tailed Student's *t* test: ** and ***, $p < 0.01$ and $p < 0.001$, respectively.

kinase inhibitor 1A (*CDKN1A*), and thioredoxin-interacting protein (*TXNIP*), were up-regulated, and five genes, cyclin B1 (*CCNB1*), cyclin-dependent kinase inhibitor 3 (*CDKN3*), cell division cycle 20 (*CDC20*), Aurora kinase A (*AURKA*), and proline and serine-rich coiled-coil 1 (*PSRC1*), were down-regulated after 10 μM 5-FU treatment for 16 h (Fig. 9B). Subsequently, we quantified these gene expressions by qRT-PCR in each cell line, and similar tendencies were indicated in all of the genes listed above (Fig. 10, A and B). Our data support the idea that 5-FU treatment leads to cell-cycle arrest between S phase and mitotic phase, particularly in S phase.

ATR inhibition enhanced efficacy of 5-FU independent of NHEJ and HR

5-FU treatment caused cell-cycle arrest in S phase, where HR repair is active for repairing DSBs. BRCA2, one of the HR repair components, plays an important role in repairing DNA damage induced by 5-FU (3). To investigate whether ATR inhibition

affects the sensitivity of 5-FU in the absence of BRCA2, surviving fractions of the Chinese hamster lung fibroblasts were measured. We found that compared with BRCA2-proficient cells, BRCA2-deficient cells were more sensitive to 5-FU in the presence of ATRi (Fig. 11A).

To further determine whether the NHEJ or HR repair pathway is more predominant against 5-FU treatment, the surviving fraction of mouse embryonic fibroblasts (MEFs) (WT; *Lig4*^{-/-}; *Rad54*^{-/-}; *Lig4*^{-/-}*Rad54*^{-/-}) was examined. All repair gene-defective cells were sensitive to 5-FU, but *Rad54*^{-/-} cells were more sensitive to 5-FU than *Lig4*^{-/-} cells. There was very little difference in the surviving fraction between *Rad54*^{-/-} cells and *Lig4*^{-/-}*Rad54*^{-/-} cells (Fig. 11B). These results suggest that HR is more crucial than NHEJ in repairing DNA damage induced by 5-FU. Subsequently, we examined the effect of 5-FU treatment combined with ATRi on the *Lig4*^{-/-}*Rad54*^{-/-} cell lines. Surviving fractions of 0.5 μM ATRi alone, 0.5 μM 5-FU alone, and 0.5 μM 5-FU combined with 0.5 μM ATRi for 24 h

Inhibition of the ATR kinase enhances 5-FU sensitivity

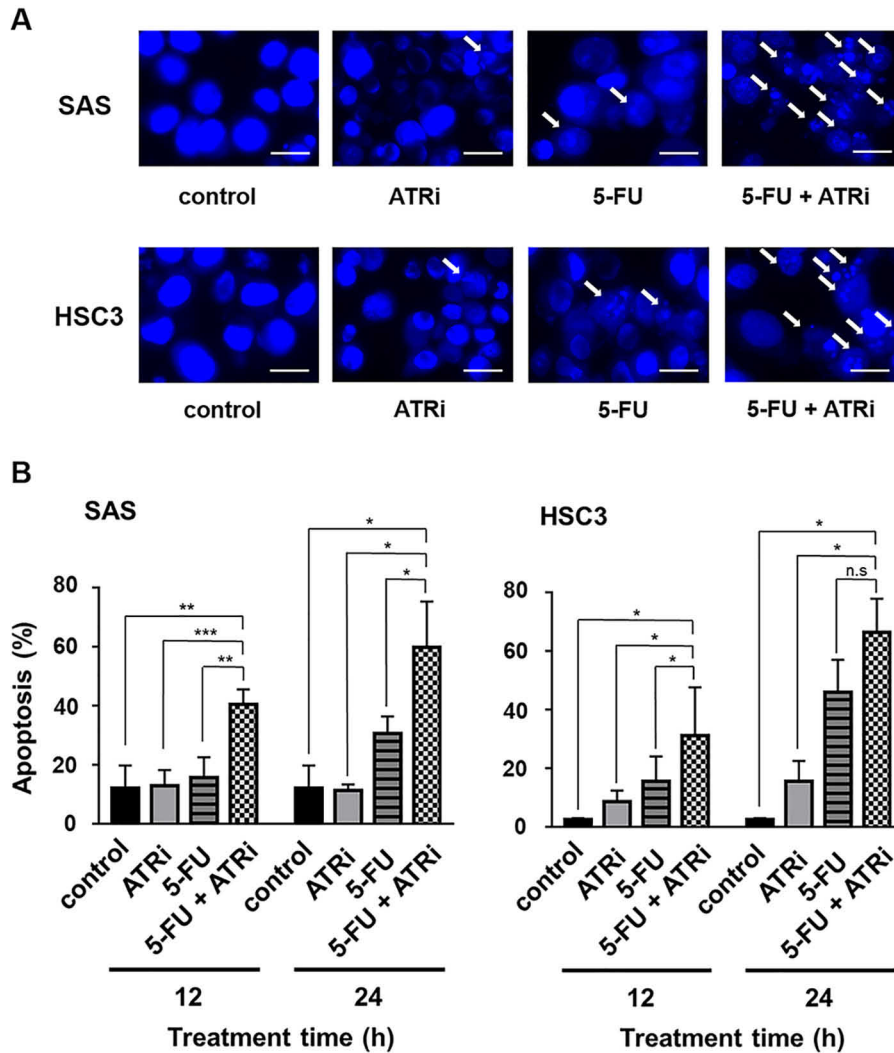


Figure 7. Apoptosis analysis by Hoechst staining. A, for morphological assessment, apoptotic cells were detected and quantified with a Hoechst33342 staining assay in SAS cells and HSC3 cells. B, cells were exposed 10 μM 5-FU and/or 3 μM ATRi for 12 h/24 h. The fraction of apoptosis was schematized as illustrated in SAS and HSC3. Bars, 20 μm . All experiments were replicated three times. The values obtained are indicated as means \pm S.D. (error bars). Data were compared statistically using the two-tailed Student's *t* test: *, **, and ***, $p < 0.05$, $p < 0.01$, and $p < 0.001$, respectively. *n.s.*, not significant.

were 85.0 ± 8.6 , 91.8 ± 3.5 , and $25.3 \pm 3.7\%$, respectively (Fig. 11C). Cell viability was remarkably decreased in the 5-FU treatment combined with ATRi compared with 5-FU alone (Fig. 11C).

Discussion

ATR is an apical signaling kinase in the replication stress response (33). ATR senses stalled replication forks and is recruited to the forks through direct interactions with the ssDNA-coated RPA at the forks, consequently preventing fork collapse and the formation of DNA breaks (34–36). Moreover, ATR is involved in S- and G₂-phase arrest by activating intra-S and G₂/M checkpoint (33) and is necessary during the HR repair pathway (37). On the other hand, 5-FU is thought to be an inhibitor of the enzyme TS, which plays a role in nucleotide synthesis (38, 39). 5-FU induces unstable conformations in the DNA structure at the S phase, and where too many SSBs are present at stalled replication forks in 5-FU-treated cells, DSBs are induced (9, 10). We consider ATR to be the principal

factor in recognizing and repairing DNA damage induced by 5-FU treatment.

There has been some debate over whether gene depletion and inhibition toward ATR are different. We considered the use of ATR kinase inhibitor to be a more feasible approach than ATR depletion by gene knockdown or knockout approaches for two reasons: 1) it is useful to study inhibitory effects using already established inhibitors that have been applied clinically or are already in clinical trials, and 2) the depletion of ATR is lethal to mammalian cells (40), whereas depletion of ATM or DNA-PK is not. Therefore, all of the experiments in this study were performed using specific kinase inhibitors.

Unrepaired DSBs are toxic to cells. Our results demonstrate that SAS cells and HSC3 cells respond differently in terms of DSB induction and cellular survival toward 5-FU and ATRi treatment. Different cells respond differently to DSBs in terms of phosphorylation of histone H2AX (41) because different cells have different DDR status. Cells also have different cell death and survival pathways (*i.e.* p53 status). Hence, it might be

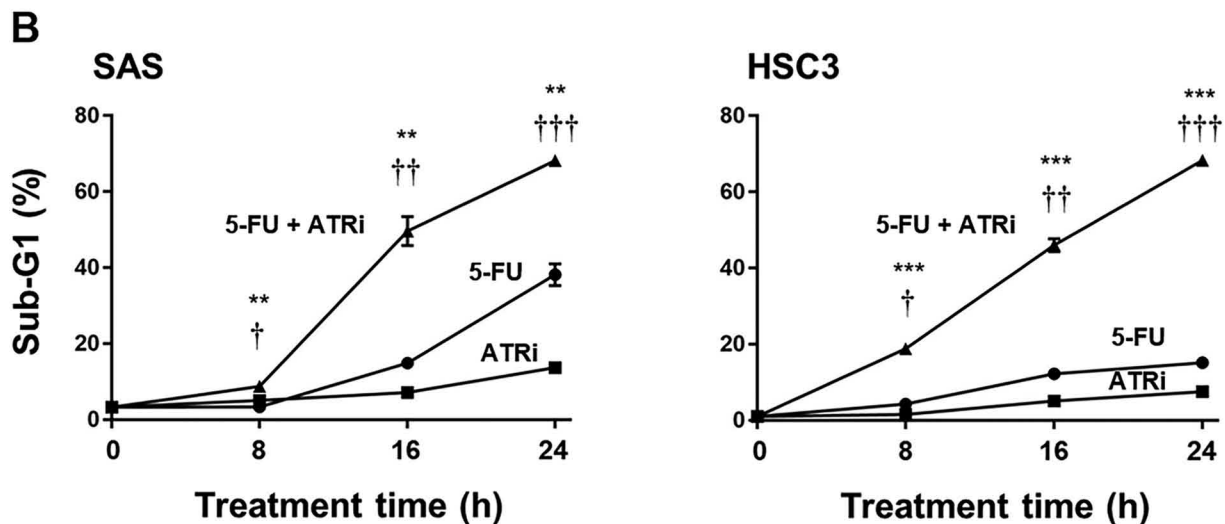
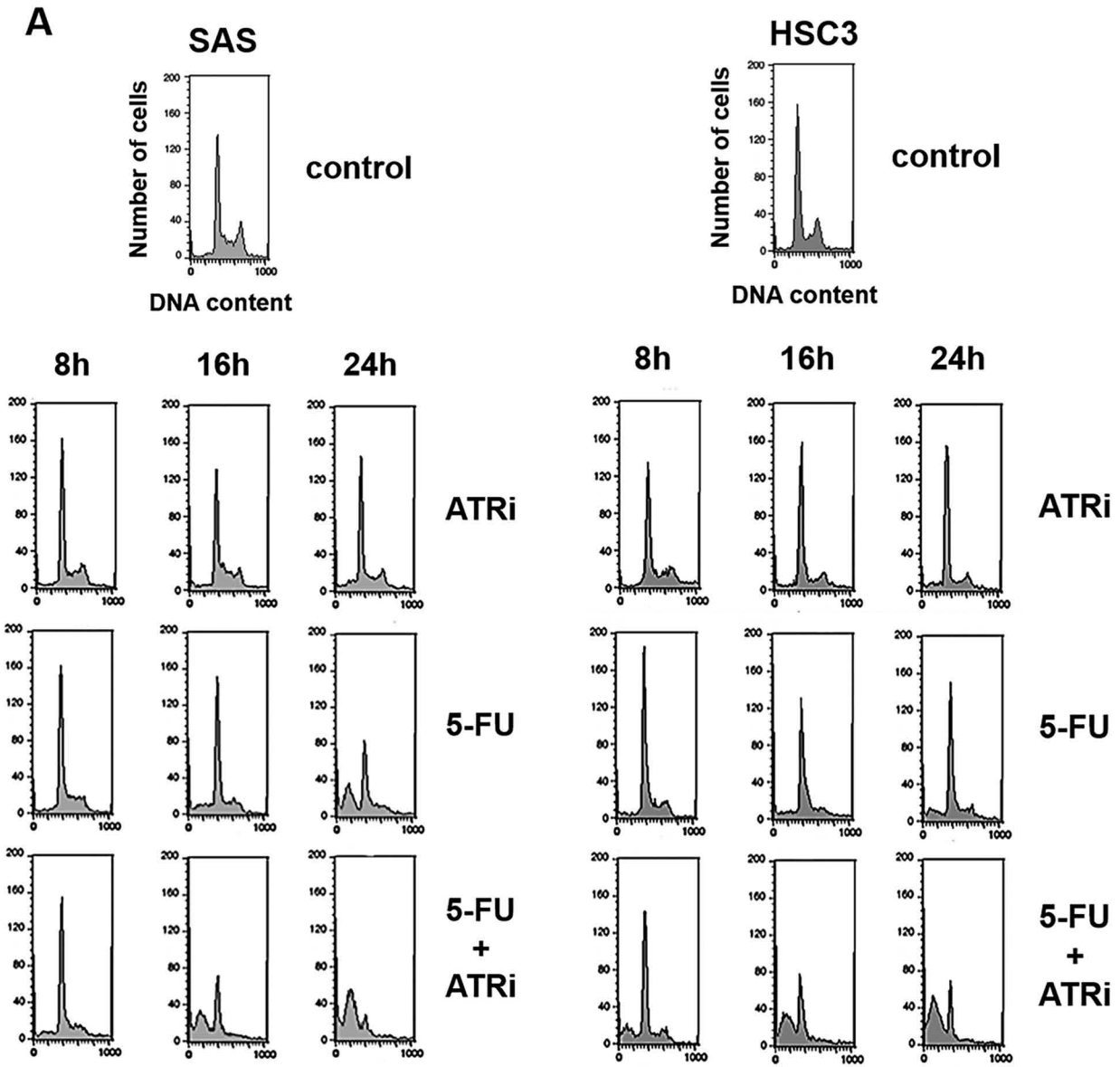
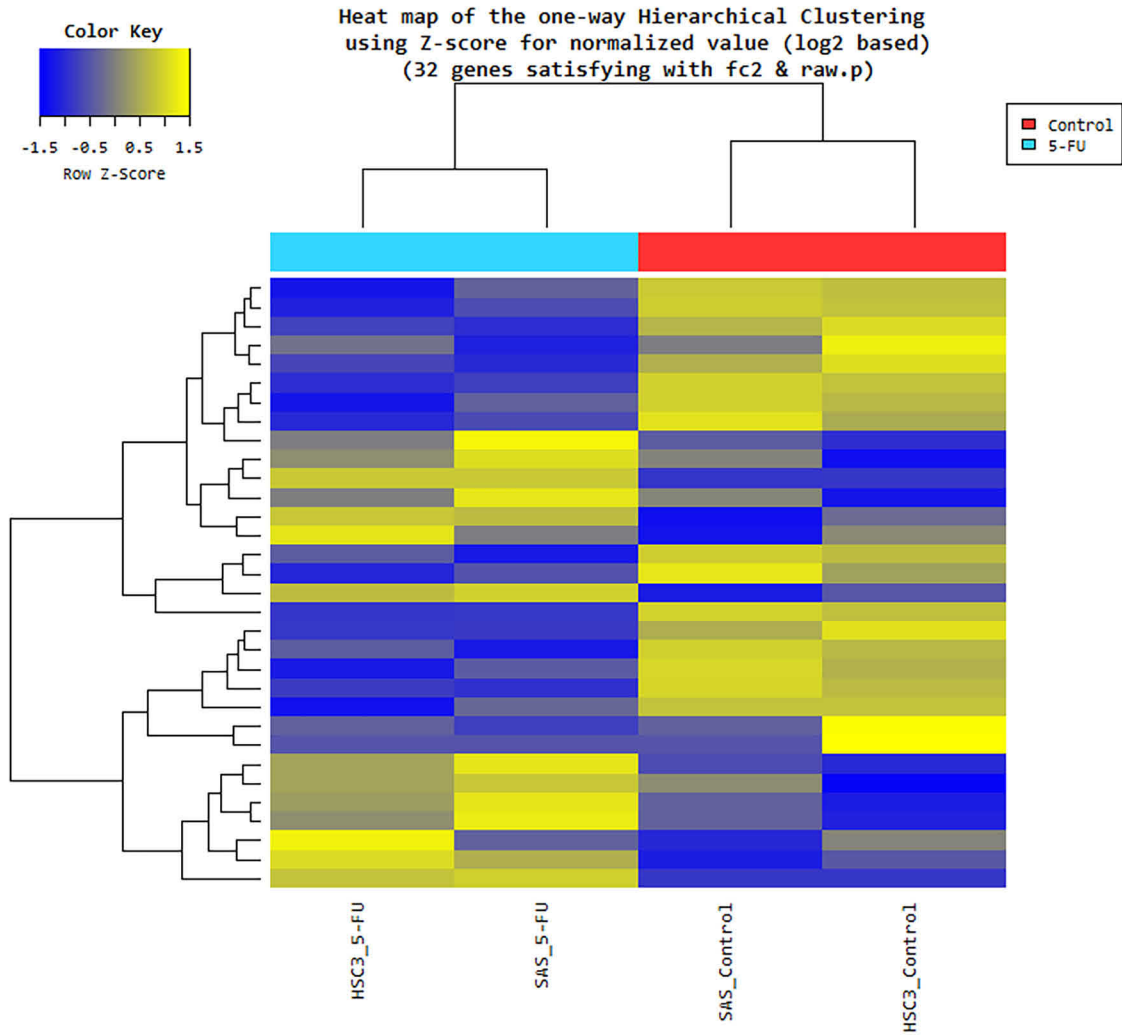


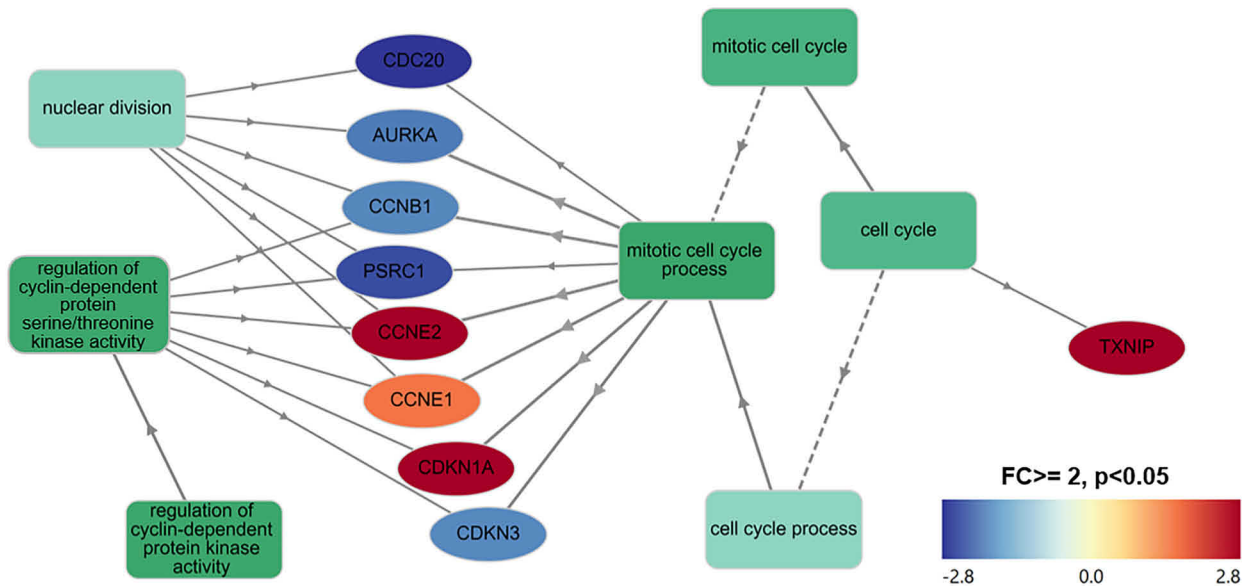
Figure 8. Apoptosis analysis by sub-G₁ accumulation. *A*, results of cell-cycle analysis after 10 μ M 5-FU and/or 3 μ M ATRi treatment for 8 h/16 h/24 h in SAS cells and HSC3 cells. *B*, sub-G₁ cells were schematized as illustrated in SAS and HSC3. All experiments were replicated three times. The values obtained are indicated as means \pm S.D. (error bars). Data were compared statistically using the two-tailed Student's *t* test: †, **/††, and ***/†††, $p < 0.05$, $p < 0.01$, and $p < 0.001$, respectively.

Inhibition of the ATR kinase enhances 5-FU sensitivity

A



B



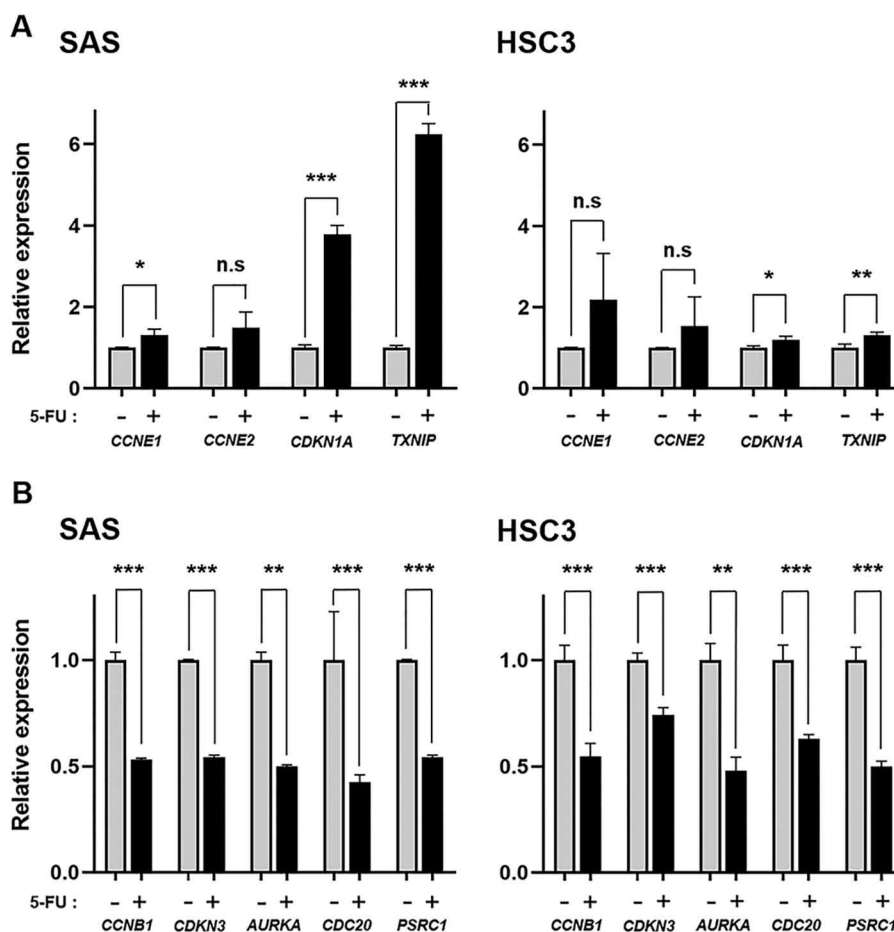


Figure 10. Gene expression analysis by qRT-PCR. A and B, quantitative qRT-PCR after 10 μM 5-FU treatment for 16 h in SAS cells and HSC3 cells. All experiments were replicated three times. The values obtained were described as means \pm S.D. (error bars). Data were compared statistically using the two-tailed Student's *t* test: *, **, and ***, $p < 0.05$, $p < 0.01$, and $p < 0.001$, respectively. n.s., not significant.

reasonable to use DSBs and DDR markers for the quantification of DNA damage and correlation of cellular survival.

To repair DNA damage accurately, the cell cycle must be arrested by a cell-cycle checkpoint to allow time for DNA repair. It was previously reported that 5-FU treatment led to S-phase arrest (9), and our results in this study showed that cells were arrested at S phase after 5-FU treatment (Fig. 8A). ATR activates the intra-S checkpoint in response to DNA damage (33), and inhibition of ATR suppresses the intra-S checkpoint, leading the cells with DNA damage to enter G₂ phase (42). Subsequently, damaged cells at G₂ phase enter mitosis by the effect of ATRi (42), and then mitotic catastrophe occurs during mitosis (43, 44). In the presence of ATRi, cells are not capable of activating the intra-S checkpoint and repairing DNA damage induced by 5-FU. Thus, cell death induced by combination of 5-FU and ATRi might be caused by mitotic catastrophe.

Based on the results of the transcriptome analysis together with qPCR, 5-FU treatment led to cell-cycle arrest between S phase and mitotic phase, especially at S phase (Figs. 9B and 10 (A and B)). CCNE (CCNE1 and CCNE2), encoded by *CCNE1*

and *CCNE2*, are involved in G₁/S transition, and its expression level gradually increases as the cell cycle transitions from G₁ phase to S phase, reaching its highest expression level immediately after entering S phase and gradually being degraded through S phase (45). Cyclin-dependent kinase (CDK) inhibitor p21 encoded by *CDKN1A* arrests the cell cycle at G₁, S, and G₂ phases by preventing cyclin-CDK complex (46–48). TXNIP encoded by *TXNIP* acts on cell-cycle arrest through retaining the p27/CDK inhibitor in the nucleus (49, 50). High expression of *CCNE1* and *CCNE2* in response to 5-FU treatment suggests that 5-FU treatment causes early S-phase arrest, and high expression of *CDKN1A* and *TXNIP* after 5-FU treatment explains why cells were arrested in S phase after 5-FU treatment (Fig. 8A). *CCNB1* encoded by *CCNB1* is involved in G₂/M transition (51), and expression of *CCNB1* increases as the G₂ phase progresses (52); thus, *CCNB1* down-regulation suggests that cells were arrested at G₂ phase in response to 5-FU treatment. Proteins encoded by *CDC20*, *AURKA*, and *PSRC1* play roles in mitosis (53–55), and the down-regulation of these three genes suggests that cells were arrested at mitotic phase in response to 5-FU treatment.

Figure 9. Transcriptome sequencing analysis. A, a heat map shows the results of hierarchical clustering analysis, which clusters the similarity of genes and samples by expression level (normalized value) from a significant list. B, GO analysis of significant expressed genes regarding cell cycle both in SAS cells and HSC3 cells after 10 μM 5-FU treatment for 16 h. Color density indicates the gene expression level.

Inhibition of the ATR kinase enhances 5-FU sensitivity

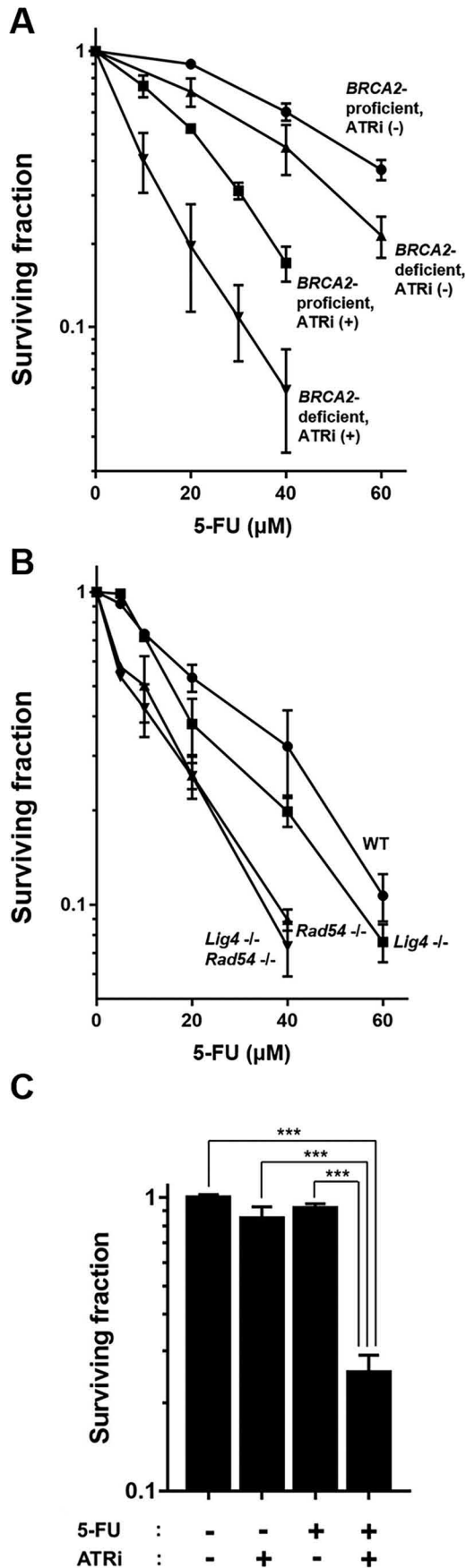


Figure 11. Contributions of NHEJ and HR repair pathways. A, surviving fraction of *BRCA2*-proficient and *BRCA2*-deficient Chinese hamster lung fibro-

blasts treated with various concentrations of 5-FU and/or 3 μM ATRi for 24 h. B, surviving fractions of MEFs WT (filled circles), *Lig4*^{-/-} (filled squares), *Rad54*^{-/-} (filled triangles), and *Lig4*^{-/-}*Rad54*^{-/-} (filled inverted triangles) treated with 5-FU for 24 h. C, surviving fraction of MEFs *Lig4*^{-/-}*Rad54*^{-/-} treated with 0.5 μM 5-FU and/or 0.5 μM ATRi for 24 h. All experiments were replicated three times. The values obtained are indicated as means \pm S.D. (error bars). Data were compared statistically using the two-tailed Student's *t* test. ***, *p* < 0.001.

ATR was reported to be recruited to centromeres in mitosis dependent on the activity of Aurora A kinase encoded by *AURKA* (56). The down-regulation of *AURKA* in response to 5-FU treatment suggests that 5-FU treatment could inhibit the localization of ATR to centromeres. ATR inhibition on top of 5-FU treatment might further compromise centromere maintenance, leading to increased cell death at mitotic phase. The autophosphorylation of ATM, an indicator of ATM activation, was induced by 5-FU treatment. However, in terms of cell killing, ATMi was not as effective as ATRi when combined with 5-FU (Fig. 2, A, B, and D). *CDKN3* encodes the downstream effector of ATM in the DSB repair pathway, which is a KRAB-associated protein (KAP-1), and KAP-1 is phosphorylated at the DSB damage site in an ATM-dependent manner (57). *CDKN3* was down-regulated in response to 5-FU, suggesting that low amounts of KAP-1 lead to deficits in the repair of DSBs conducted by ATM even though ATM was activated by 5-FU treatment. Moreover, ATM and MRE11 stimulate the ATR signaling pathway by converting DNA damage into structures that recruit and activate ATR (58). Even when ATM is inhibited by ATMi, 5-FU-induced DNA damage activates ATR to repair and respond, thus leading to survival.

5-FU causes more SSB accumulation at stalled replication forks and the collapse of more forks to generate DSBs in the presence of ATRi. These DSBs would rely on *BRCA2*-dependent HR for repair. *BRCA2* mutant cells are sensitive to ATRi (59). So *BRCA2*-deficient cells are expected to be more sensitive to 5-FU combined with ATRi. Indeed, the fraction of cytotoxicity of ATRi in *BRCA2*-deficient cells was more sensitive than that in *BRCA2*-proficient cells (Fig. 11A), even though *BRCA2* is downstream of ATR (25–28). Our data suggest that DNA damage induced by 5-FU treatment could also be repaired in an ATR-dependent manner but by mechanisms other than the conventional HR repair pathway.

In the case of ATR inhibition using *Lig4/Rad54*-knockout cells, neither HR nor NHEJ was involved in the repair of 5-FU-induced DNA lesions. It is conceivable that the SSB repair pathway, like BER and MMR, would be responsible for the repair of 5-FU-induced DNA damage in the absence of both NHEJ and HR repair pathways. The significant difference of cell survival between 5-FU treatment alone and 5-FU combined with ATRi might not only be due to ATRi suppression of SSBs repair but also its impact on molecular mechanisms other than DNA repair.

ATR inhibition using *BRCA2*-deficient cells and *Lig4/Rad54*-knockout cells demonstrates that ATR is involved in DNA repair other than NHEJ and HR (Fig. 11, A–C). ATR responds to a wide range of DNA damage and DNA replication stress (60), and it is required for telomere maintenance through alternative lengthening of telomeres (61). In

addition, ATR plays key roles in the suppression of chromosome instability at centromeres through the promotion of faithful chromosome segregation (56). 5-FU treatment combined with ATRi is effective on cell killing because ATR inhibition not only blocks DNA repair pathways but also affects other intracellular dynamics, such as chromosome maintenance through telomeres and centromeres.

The results in our current study suggest that ATR inhibition is a potential therapeutic approach to enhance 5-FU treatment on cancer cells. With different *p53* status, they are dependent not only on the HR repair pathway but also on other DNA repair pathways. For future therapeutic efforts, the application of ATR inhibitor may prove to be an effective tool in enhancing the efficacy of 5-FU chemotherapy for cancer patients. Subsequent studies will be required to further elucidate the mechanism of DDR and the repair of 5-FU-induced DNA damage.

Experimental procedures

Cell lines

The present study used SAS (*p53*-proficient) and HSC3 (*p53*-deficient) human oral squamous cell carcinoma cell lines obtained from the Japanese Collection of Research Bioresources (Health Science Research Resources Bank, Osaka, Japan). SAS cells express WT *p53* protein (62–64). HSC3 cells are impaired to express *p53* protein (65). Chinese hamster lung fibroblasts used were V79 (*BRCA2*-proficient) and V-C8 (*BRCA2*-deficient), kindly provided by Dr. M. Z. Zdzienicka. The cell lines used were MEFs *Lig4*^{+/+}*Rad54*^{+/+}*p53*^{-/-} (WT); *Lig4*^{-/-}*Rad54*^{+/+}*p53*^{-/-} (*Lig4*^{-/-}); *Lig4*^{+/+}*Rad54*^{-/-}*p53*^{-/-} (*Rad54*^{-/-}); *Lig4*^{-/-}*Rad54*^{-/-}*p53*^{-/-} (*Lig4*^{-/-}*Rad54*^{-/-}), kindly provided by Dr. F. W. Alt. Cells were cultured at 37 °C in Dulbecco's modified Eagle's medium containing 10% (v/v) fetal bovine serum, penicillin (50 units/ml), and streptomycin (50 µg/ml) (DMEM-10).

Chemicals and chemical treatment

5-FU (Kyowa Hakko, Tokyo, Japan), ATR inhibitor VE-821 (Selleck Chemicals, Houston, TX, USA), DNA-PK inhibitor NU7441 (KU57788) (TOCRIS, Bristol, UK), and ATM inhibitor KU55933 (TOCRIS) were used either on their own or in combination. A medium containing 5-FU at various concentrations was used to treat cells with respective inhibitors over a range of 8–24 h before the cells were rinsed twice with PBS.

Western blotting

Total protein from SAS cells treated with 5-FU and/or ATRi for 24 h were isolated using radioimmune precipitation assay lysis buffer containing protease and phosphatase inhibitor mixture and quantified by the Protein Assay Bicinchoninate Acid (BCA) kit (Nacalai Tesque, Kyoto, Japan). Isolated proteins (30 µg) were separated by 4–15% SDS-PAGE and transferred onto polyvinylidene difluoride membranes. The membranes were probed overnight at 4 °C using the following antibodies: anti-phospho-ATR (Thr-1989; GTX128145, GeneTex, Los Angeles, CA, USA), anti-ATR (A300-138A, Bethyl, Montgomery, AL, USA), anti-phospho-ATM (Ser-1981; catalog no. 13050, Cell

Signaling Technology, Danvers, MA, USA), anti-ATM (A300-299A, Bethyl), anti-phospho-DNA-PKcs (Ser-2056; ab124918, Abcam, Cambridge, UK), anti-DNA-PKcs (3H6; catalog no. 123111, Cell Signaling Technology), anti-phospho-Chk1 (Ser-345; catalog no. 2341, Cell Signaling Technology), anti-Chk1 (G-4; SC-8408, Santa Cruz Biotechnology, Inc., Dallas, TX, USA), anti-p53 (DO-1; SC-126, Santa Cruz Biotechnology), and anti-β-actin (Wako, Osaka, Japan). Blots were visualized using an enhanced chemiluminescence method (Bio-Rad) according to the manufacturer's protocol.

Colony-forming assays

We measured cell survival using a standard colony-forming assay. In each experiment, three flasks were used, and three independent experiments were performed at each survival point. Colonies obtained after 7–10 days were fixed with methanol and stained with a 2% Giemsa solution. Microscopic colonies containing ~50 cells were scored as having grown from single surviving cells.

DSB analysis by neutral comet assay

The neutral single-cell gel electrophoresis (comet) assay was performed using the Comet Assay Kit (CELL BIOLABS, San Diego, CA, USA). The treated cells were resuspended at 10⁵ cells/ml in ice-cold PBS. Combined cell samples with Comet-agarose at a 1:10 ratio, mixed well by pipetting, were immediately transferred to 75 µl/well. The slide was then transferred to a prechilled lysis buffer for 30 min and then transferred to a prechilled alkaline solution for 30 min. It was subsequently immersed in prechilled neural TBE electrophoresis solution. Voltage was applied to the immersed slide for 15 min at 1 V/cm. After electrophoresis, the slide was stained with 1:10,000 diluted Vista Green DNA Dye. Nuclei were observed under a fluorescence microscope. Each comet tail moment was quantified using ImageJ (66).

H2AX phosphorylation analysis by immunocytochemistry

Cells were grown on glass slides in 6-well plates, fixed in 2% paraformaldehyde in PBS for 15 min at room temperature. We permeabilized the cells for 5 min at 4 °C in 0.2% Triton X-100, and they were blocked in PBS with 1% bovine serum albumin (BSA) for 1 h at 37 °C. They were then incubated with anti-phospho-H2AX (Ser-139) mouse mAb (Upstate Biotechnology, Inc., Lake Placid, NY, USA) for 1 h at 1:300 dilutions in PBS containing 1% BSA and washed three times in PBS containing 1% BSA for 10 min. The cells were incubated with Alexa Fluor 488-conjugated anti-mouse second antibody (Molecular Probes, Inc., Eugene, OR, USA) for 1 h at room temperature at 1:400 dilutions in PBS containing 1% BSA and washed three times for 10 min in PBS. Coverglasses were mounted at 1:1000 dilutions of 4',6-diamidino-2-phenylindole. Fluorescent images were captured for analysis using an FV3000 confocal microscope (Olympus). Histone H2AX phosphorylation foci were quantified using ImageJ (66). A mean intensity of ≥100 arbitrary units/cell was considered as pan-nuclear-positive.

Inhibition of the ATR kinase enhances 5-FU sensitivity

H2AX phosphorylation analysis by flow cytometry

Cells were fixed in cold 70% methanol after a 10 μM 5-FU with or without ATRi (3 μM) treatment for 6 and 12 h and maintained at 4 °C for up to 1 week before analysis. The overall levels of phosphorylated H2AX (γH2AX) were measured with flow cytometry.

Analysis of apoptosis by Hoechst staining

Detection of apoptotic bodies with a Hoechst33342 staining assay was used to analyze the induction of apoptosis. Cells were fixed with 1% glutaraldehyde (Nacalai Tesque, Kyoto Japan) in PBS at 4 °C, washed with PBS, stained with 0.2 mM Hoechst33342 (Nacalai Tesque), and then observed under a fluorescence microscope.

Analysis of apoptosis by flow cytometry

After 5-FU and/or ATRi treatment, cells were fixed with cold 70% methanol and stored at 4 °C for 3 days prior to analysis. To analyze the cell cycle, cells were incubated for 30 min at room temperature with 1 mg/ml RNase and 50 $\mu\text{g}/\text{ml}$ propidium iodide and analyzed using a flow cytometer. Cell-cycle distribution was then assayed by determining the DNA content twice and deriving its average values.

Transcriptome sequencing analysis

Total RNA from SAS and HSC3 cells was isolated according to the protocol specified in the Purelink RNA minikit (Thermo Fisher Scientific, Waltham, MA, USA). We pooled three replicated samples of each RNA into one sample. We used a DU730 UV-visible spectrophotometer (Beckman Coulter, Brea, CA, USA) to measure the concentration and purity of the RNA samples. Contamination DNA was eliminated using DNase. RNA was purified randomly fragment for short read sequencing and then reverse-transcribed into cDNA. Adapters were ligated onto both ends of the cDNA fragments. After fragments were amplified using PCR, fragments were selected with insert sizes between 200 and 400 bp. For paired-end sequencing, both ends of the cDNA were sequenced by the read length. The quality control of the sequenced raw reads was analyzed. Trimmed reads were mapped to the reference genome with HISAT2 (67, 68), a splice-aware aligner. The transcript was assembled by StringTie (68, 69) with aligned reads. Expression profiles are indicated as read count and normalization value, which is based on transcript length and depth of coverage. In groups with different conditions, genes or transcripts that express differentially were filtered out through statistical hypothesis testing. Statistical analysis was performed using $-\log_{10}$ fold change, exactTest (70) using edgeR (71) per comparison pair. The significant results were selected on conditions of $|fc| \geq 2$ and raw p value < 0.05 . In cases of known gene annotation, functional annotation and gene-enrichment analysis were performed using GOnet (72) based on the GO (<http://geneontology.org/>) database.

Quantitative PCR

RNA from SAS and HSC3 cells was extracted according to the protocol specified in the Purelink RNA minikit (Thermo Fisher Scientific). We used a DU730 UV-visible spectrophotometer (Beckman Coulter) to measure the concentration and purity of the RNA samples. Extracted RNA (0.5 μg) was reverse-transcribed based on the protocol outlined in the ReverTra Ace qPCR RT Master Mix (TOYOBO, Osaka, Japan). The StepOne Plus Real-time PCR System (Thermo Fisher Scientific) was used to amplify and quantify levels of target gene cDNA. We performed qRT-PCR with SsoAdvanced Universal SYBR Green Supermix (Bio-Rad) and specific primers for qRT-PCR. We also ran reactions in triplicate and normalized the expression of each gene to the geometric mean of β -actin as a housekeeping gene and applied the $\Delta\Delta\text{CT}$ method for analysis. The following primers were designed by Bio-Rad: CCNE1 (qHsaCID0015131), CCNE2 (qHsaCID0007224), CCNB1 (qHsaCED0044529), CDKN1A (qHsaCID0014498), CDKN3 (qHsaCID0010035), CDC20 (qHsaCID0012637), AURKA (qHsaCID0022123), TXNIP (qHsaCED0043730), PSRC1 (qHsaCED0038868), and β -actin (qHsaCED0036269).

Statistical analysis

The values obtained are indicated as means \pm S.D. Data were compared statistically using the two-tailed Student's t test; $^*/t$, $^{**}/t$, and $^{***}/t$ represent $p < 0.05$, $p < 0.01$, and $p < 0.001$, respectively.

Data availability

The bulk RNA-Seq reads have been submitted to the DDBJ Sequence Read Archive (DRA) under accession number [DRA010063](https://www.ddbj.go.jp/DRASearch/DRASearch.html).

Acknowledgments—We thank Dr. Takeo Ohnishi for guidance of and support for this project over the years, Keren-Happuch E and Dr. Takahiko Nakagawa for critical reading of the manuscript, and Drs. M. Z. Zdzienicka and F. W. Alt. for kindly providing the cell lines used in this work.

Author contributions—S. S. I., Y. N., A. K., M. H., E. M., and T. K. conceptualization; S. S. I., Y. N., M. M., Y. M. S., S. Kobashigawa, H. N., M. N., F. K., and S. Kikuchi data curation; S. S. I., Y. N., M. M., Y. M. S., S. Kobashigawa, T. K. M., H. N., M. N., S. Kikuchi, K. S., and G. K. formal analysis; S. S. I., Y. N., Y. M. S., S. Kobashigawa, M. H., E. M., and T. K. validation; S. S. I., Y. N., M. M., Y. M. S., S. Kobashigawa, and F. K. investigation; S. S. I., K. S., G. K., M. H., E. M., and T. K. visualization; S. S. I., M. H., E. M., and T. K. writing-original draft; S. S. I., Y. N., A. T., M. H., E. M., and T. K. project administration; S. S. I., Y. N., M. M., Y. M. S., S. Kobashigawa, T. K. M., H. N., M. N., F. K., S. Kikuchi, A. K., S. T., K. S., G. K., A. T., M. H., E. M., and T. K. writing-review and editing; Y. N., M. N., A. K., S. T., K. S., G. K., A. T., M. H., E. M., and T. K. resources; Y. N., S. Kobashigawa, T. K. M., H. N., M. N., S. Kikuchi, M. H., E. M., and T. K. funding acquisition; M. H., E. M., and T. K. supervision.

Funding and additional information—This work was supported by Japan Society for the Promotion of Science (JSPS) KAKENHI Grants JP18K17234 (to Y. N.), JP20H03199 (to E. M.), JP19K08150 (to S. Kobashigawa), JP19K23976 (to M. N.), JP19K21306 and JP20K16583 (to H. N.), JP18K07764 (to G. K.), and JP19K10272 (to T. K.) and AMED Brain/MINDS Beyond Grant JP20dm0307032 (to E. M.). This work was also supported by grants from the Takeda Science Foundation (to E. M. and T. K. M.), Kanzawa Medical Research Foundation (to E. M.), Uehara Memorial Foundation (to E. M. and S. Kikuchi), Nakatomi Foundation (to E. M.), Konica Minolta Science and Technology Foundation (to E. M.), Naito Foundation (to E. M.), MSD Life Science Foundation (to E. M.), Mochida Memorial Foundation for Medical and Pharmaceutical Research (to E. M.), SENSHIN Medical Research Foundation (to E. M.), Terumo Foundation for Life Sciences and Arts (to E. M.), Nara Kidney Disease Research Foundation (to E. M.), Novartis Research (to E. M. and H. N.), Sumitomo Dainippon Pharma Research (to T. K. M.), and Tokyo Biochemical Research Foundation (to S. Kikuchi) and unrestricted funds from Dr. Taichi Noda (KTX Corp., Aichi, Japan) and Dr. Yasuhiro Horii (Koseikan, Nara, Japan) (to E. M.).

Conflict of interest—The authors declare that they have no conflicts of interest with the contents of this article.

Abbreviations—The abbreviations used are: 5-FU, 5-fluorouracil; ATR, ataxia telangiectasia mutated and Rad3-related protein; DSB, double-strand break; NHEJ, nonhomologous end joining; HR, homologous recombination; SSB, single-strand break; ATM, ataxia telangiectasia mutated protein; DNA-PK, DNA-dependent protein kinase; DNA-PKcs, DNA-PK catalytic subunit; Chk1, checkpoint kinase 1; BRCA2, breast cancer susceptibility gene 2; CCNB1, cyclin B1; CCNE1, cyclin E1; CCNE2, cyclin E2; CDKN1A, cyclin-dependent kinase inhibitor 1A; CDKN3, cyclin-dependent kinase inhibitor 3; CDC20, cell division cycle 20; AURKA, Aurora kinase A; TXNIP, thioredoxin-interacting protein; PSRC1, proline and serine-rich coiled-coil 1; MEF, mouse embryonic fibroblast; KAP-1, KRAB-associated protein; FdUTP, fluorodeoxyuridine triphosphate; FdUMP, fluorodeoxyuridine monophosphate; TS, thymidylate synthase; BER, base excision repair; MMR, mismatch repair; DDR, DNA damage response; ATRi, ATR inhibitor; DNA-PKi, DNA-PK inhibitor; ATMi, ATM inhibitor; GO, gene ontology; qRT-PCR, quantitative PCR; CDK, cyclin-dependent kinase.

References

- Longley, D. B., Harkin, D. P., and Johnston, P. G. (2003) 5-fluorouracil: mechanisms of action and clinical strategies. *Nat. Rev. Cancer* **3**, 330–338 [CrossRef Medline](#)
- Miura, K., Kinouchi, M., Ishida, K., Fujibuchi, W., Naitoh, T., Ogawa, H., Ando, T., Yazaki, N., Watanabe, K., Haneda, S., Shibata, C., and Sasaki, I. (2010) 5-FU metabolism in cancer and orally-administrable 5-FU drugs. *Cancers* **2**, 1717–1730 [CrossRef Medline](#)
- Nakagawa, Y., Kajihara, A., Takahashi, A., Kondo, N., Mori, E., Kirita, T., and Ohnishi, T. (2014) The BRCA2 gene is a potential molecular target during 5-fluorouracil therapy in human oral cancer cells. *Oncol. Rep.* **31**, 2001–2006 [CrossRef Medline](#)
- Wyatt, M. D., and Wilson, D. M. (2009) Participation of DNA repair in the response to 5-fluorouracil. *Cell Mol. Life Sci.* **66**, 788–799 [CrossRef Medline](#)
- Li, L. S., Morales, J. C., Veigl, M., Sedwick, D., Greer, S., Meyers, M., Wagner, M., Fishel, R., and Boothman, D. A. (2009) DNA mismatch repair (MMR)-dependent 5-fluorouracil cytotoxicity and the potential for new therapeutic targets. *Br. J. Pharmacol.* **158**, 679–692 [CrossRef Medline](#)
- Fischer, F., Baerenfaller, K., and Jiricny, J. (2007) 5-Fluorouracil is efficiently removed from DNA by the base excision and mismatch repair systems. *Gastroenterology* **133**, 1858–1868 [CrossRef Medline](#)
- Das, D., Preet, R., Mohapatra, P., Satapathy, S. R., Siddharth, S., Tamir, T., Jain, V., Bharatam, P. V., Wyatt, M. D., and Kundu, C. N. (2014) 5-Fluorouracil mediated anti-cancer activity in colon cancer cells is through the induction of adenomatous polyposis coli: implication of the long-patch base excision repair pathway. *DNA Repair (Amst.)* **24**, 15–25 [CrossRef Medline](#)
- Lindahl, T. (1974) An *N*-glycosidase from *Escherichia coli* that releases free uracil from DNA containing deaminated cytosine residues. *Proc. Natl. Acad. Sci. U. S. A.* **71**, 3649–3653 [CrossRef Medline](#)
- Fujinaka, Y., Matsuoka, K., Iimori, M., Tuul, M., Sakasai, R., Yoshinaga, K., Saeki, H., Morita, M., Kakeji, Y., Gillespie, D. A., Yamamoto, K., Takata, M., Kitao, H., and Maehara, Y. (2012) ATR-Chk1 signaling pathway and homologous recombinational repair protect cells from 5-fluorouracil cytotoxicity. *DNA Repair (Amst.)* **11**, 247–258 [CrossRef Medline](#)
- Zhang, X. P., Liu, F., Cheng, Z., and Wang, W. (2009) Cell fate decision mediated by p53 pulses. *Proc. Natl. Acad. Sci. U. S. A.* **106**, 12245–12250 [CrossRef Medline](#)
- Maréchal, A., and Zou, L. (2013) DNA damage sensing by the ATM and ATR kinases. *Cold Spring Harb. Perspect. Biol.* **5**, a012716 [CrossRef Medline](#)
- Woods, D., and Turchi, J. J. (2013) Chemotherapy induced DNA damage response: convergence of drugs and pathways. *Cancer Biol. Ther.* **14**, 379–389 [CrossRef Medline](#)
- Heffernan, T. P., Simpson, D. A., Frank, A. R., Heinloth, A. N., Paules, R. S., Cordeiro-Stone, M., and Kaufmann, W. K. (2002) An ATR- and Chk1-dependent S checkpoint inhibits replicon initiation following UVC-induced DNA damage. *Mol. Cell Biol.* **22**, 8552–8561 [CrossRef Medline](#)
- Borges, H. L., Linden, R., and Wang, J. Y. (2008) DNA damage-induced cell death: lessons from the central nervous system. *Cell Res.* **18**, 17–26 [CrossRef Medline](#)
- Goto, H., Natsume, T., Kanemaki, M. T., Kaito, A., Wang, S., Gabazza, E. C., Inagaki, M., and Mizoguchi, A. (2019) Chk1-mediated Cdc25A degradation as a critical mechanism for normal cell cycle progression. *J. Cell Sci.* **132**, jcs223123 [CrossRef Medline](#)
- Buisson, R., Boisvert, J. L., Benes, C. H., and Zou, L. (2015) Distinct but concerted roles of ATR, DNA-PK, and Chk1 in countering replication stress during S phase. *Mol. Cell* **59**, 1011–1024 [CrossRef Medline](#)
- Jackson, S. P. (2002) Sensing and repairing DNA double-strand breaks. *Carcinogenesis* **23**, 687–696 [CrossRef Medline](#)
- Kanaar, R., Hoeijmakers, J. H., and van Gent, D. C. (1998) Molecular mechanisms of DNA double strand break repair. *Trends Cell Biol.* **8**, 483–489 [CrossRef Medline](#)
- Rothkamm, K., Krüger, I., Thompson, L. H., and Löbrich, M. (2003) Pathways of DNA double-strand break repair during the mammalian cell cycle. *Mol. Cell Biol.* **23**, 5706–5715 [CrossRef Medline](#)
- Hinz, J. M., Yamada, N. A., Salazar, E. P., Tebbs, R. S., and Thompson, L. H. (2005) Influence of double-strand-break repair pathways on radio-sensitivity throughout the cell cycle in CHO cells. *DNA Repair (Amst.)* **4**, 782–792 [CrossRef Medline](#)
- Thompson, L. H., and Schild, D. (2001) Homologous recombinational repair of DNA ensures mammalian chromosome stability. *Mutat. Res.* **477**, 131–153 [CrossRef Medline](#)
- Davies, A. A., Masson, J. Y., McIlwraith, M. J., Stasiak, A. Z., Stasiak, A., Venkitaraman, A. R., and West, S. C. (2001) Role of BRCA2 in control of the RAD51 recombination and DNA repair protein. *Mol. Cell* **7**, 273–282 [CrossRef Medline](#)
- Ottini, L., Masala, G., D'Amico, C., Mancini, B., Saieva, C., Aceto, G., Gestri, D., Vezzosi, V., Falchetti, M., De Marco, M., Paglierani, M., Cama, A., Bianchi, S., Mariani-Costantini, R., and Palli, D. (2003) BRCA1 and BRCA2 mutation status and tumor characteristics in male breast cancer: a population-based study in Italy. *Cancer Res.* **63**, 342–347 [Medline](#)
- Schrader, K. A., Hurlburt, J., Kalloger, S. E., Hansford, S., Young, S., Huntsman, D. G., Gilks, C. B., and McAlpine, J. N. (2012) Germline BRCA1 and

Inhibition of the ATR kinase enhances 5-FU sensitivity

- BRCA2 mutations in ovarian cancer: utility of a histology-based referral strategy. *Obstet. Gynecol.* **120**, 235–240 [CrossRef](#) [Medline](#)
25. Matsuoka, S., Ballif, B. A., Smogorzewska, A., McDonald, E. R., Hurov, K. E., Luo, J., Bakalarski, C. E., Zhao, Z., Solimini, N., Lerenthal, Y., Shiloh, Y., Gygi, S. P., and Elledge, S. J. (2007) ATM and ATR substrate analysis reveals extensive protein networks responsive to DNA damage. *Science* **316**, 1160–1166 [CrossRef](#) [Medline](#)
26. Gatei, M., Zhou, B. B., Hobson, K., Scott, S., Young, D., and Khanna, K. K. (2001) Ataxia telangiectasia mutated (ATM) kinase and ATM and Rad3 related kinase mediate phosphorylation of Brca1 at distinct and overlapping sites: *in vivo* assessment using phospho-specific antibodies. *J. Biol. Chem.* **276**, 17276–17280 [CrossRef](#) [Medline](#)
27. Fradet-Turcotte, A., Sitz, J., Grapton, D., and Orthwein, A. (2016) BRCA2 functions: from DNA repair to replication fork stabilization. *Endocr. Relat. Cancer* **23**, T1–T17 [CrossRef](#) [Medline](#)
28. Venkataraman, A. R. (2001) Functions of BRCA1 and BRCA2 in the biological response to DNA damage. *J. Cell Sci.* **114**, 3591–3598 [Medline](#)
29. Liu, S., Shiotani, B., Lahiri, M., Maréchal, A., Tse, A., Leung, C. C., Glover, J. N., Yang, X. H., and Zou, L. (2011) ATR autophosphorylation as a molecular switch for checkpoint activation. *Mol. Cell* **43**, 192–202 [CrossRef](#) [Medline](#)
30. Takahashi, A., and Ohnishi, T. (2005) Does γ H2AX foci formation depend on the presence of DNA double strand breaks? *Cancer Lett.* **229**, 171–179 [CrossRef](#) [Medline](#)
31. Darzynkiewicz, Z., Bruno, S., Del Bino, G., Gorczyca, W., Hotz, M. A., Lassota, P., and Traganos, F. (1992) Features of apoptotic cells measured by flow cytometry. *Cytometry* **13**, 795–808 [CrossRef](#) [Medline](#)
32. Bedner, E., Li, X., Gorczyca, W., Melamed, M. R., and Darzynkiewicz, Z. (1999) Analysis of apoptosis by laser scanning cytometry. *Cytometry* **35**, 181–195 [CrossRef](#) [Medline](#)
33. Saldívar, J. C., Cortez, D., and Cimprich, K. A. (2017) The essential kinase ATR: ensuring faithful duplication of a challenging genome. *Nat. Rev. Mol. Cell Biol.* **18**, 622–636 [CrossRef](#) [Medline](#)
34. Smith, J., Tho, L. M., Xu, N., and Gillespie, D. A. (2010) The ATM-Chk2 and ATR-Chk1 pathways in DNA damage signaling and cancer. *Adv. Cancer Res.* **108**, 73–112 [CrossRef](#) [Medline](#)
35. Feijoo, C., Hall-Jackson, C., Wu, R., Jenkins, D., Leitch, J., Gilbert, D. M., and Smythe, C. (2001) Activation of mammalian Chk1 during DNA replication arrest: a role for Chk1 in the intra-S phase checkpoint monitoring replication origin firing. *J. Cell Biol.* **154**, 913–923 [CrossRef](#) [Medline](#)
36. Cortez, D. (2015) Preventing replication fork collapse to maintain genome integrity. *DNA Repair (Amst.)* **32**, 149–157 [CrossRef](#) [Medline](#)
37. Sirbu, B. M., and Cortez, D. (2013) DNA damage response: three levels of DNA repair regulation. *Cold Spring Harb. Perspect. Biol.* **5**, a012724 [CrossRef](#) [Medline](#)
38. Welsh, S. J., Hobbs, S., and Aherne, G. W. (2003) Expression of uracil DNA glycosylase (UDG) does not affect cellular sensitivity to thymidylate synthase (TS) inhibition. *Eur. J. Cancer* **39**, 378–387 [CrossRef](#)
39. Koehler, S. E., and Ladner, R. D. (2004) Small interfering RNA-mediated suppression of dUTPase sensitizes cancer cell lines to thymidylate synthase inhibition. *Mol. Pharmacol.* **66**, 620–626 [CrossRef](#) [Medline](#)
40. Casper, A. M., Nghiem, P., Arlt, M. F., and Glover, T. W. (2002) ATR regulates fragile site stability. *Cell* **111**, 779–789 [CrossRef](#) [Medline](#)
41. Takahashi, A., Mori, E., Somakos, G. I., Ohnishi, K., and Ohnishi, T. (2008) Heat induces γ H2AX foci formation in mammalian cells. *Mutat. Res.* **656**, 88–92 [CrossRef](#) [Medline](#)
42. Qiu, Z., Oleinick, N. L., and Zhang, J. (2018) ATR/CHK1 inhibitors and cancer therapy. *Radiother. Oncol.* **126**, 450–464 [CrossRef](#) [Medline](#)
43. Mc Gee, M. M. (2015) Targeting the mitotic catastrophe signaling pathway in cancer. *Mediators Inflamm.* **2015**, 146282 [CrossRef](#) [Medline](#)
44. Nitta, M., Kobayashi, O., Honda, S., Hirota, T., Kuninaka, S., Marumoto, T., Ushio, Y., and Saya, H. (2004) Spindle checkpoint function is required for mitotic catastrophe induced by DNA-damaging agents. *Oncogene* **23**, 6548–6558 [CrossRef](#) [Medline](#)
45. Clurman, B. E., Sheaff, R. J., Thress, K., Groudine, M., and Roberts, J. M. (1996) Turnover of cyclin E by the ubiquitin-proteasome pathway is regulated by cdk2 binding and cyclin phosphorylation. *Genes Dev.* **10**, 1979–1990 [CrossRef](#) [Medline](#)
46. Niculescu, A. B., Chen, X., Smeets, M., Hengst, L., Prives, C., and Reed, S. I. (1998) Effects of p21^{Cip1/Waf1} at both the G₁/S and the G₂/M cell cycle transitions: pRb is a critical determinant in blocking DNA replication and in preventing endoreduplication. *Mol. Cell Biol.* **18**, 629–643 [CrossRef](#) [Medline](#)
47. Ogryzko, V. V., Wong, P., and Howard, B. H. (1997) WAF1 retards S-phase progression primarily by inhibition of cyclin-dependent kinases. *Mol. Cell Biol.* **17**, 4877–4882 [CrossRef](#) [Medline](#)
48. Radhakrishnan, S. K., Feliciano, C. S., Najmabadi, F., Haegebarth, A., Kandel, E. S., Tyner, A. L., and Gartel, A. L. (2004) Constitutive expression of E2F-1 leads to p21-dependent cell cycle arrest in S phase of the cell cycle. *Oncogene* **23**, 4173–4176 [CrossRef](#) [Medline](#)
49. Russo, A. A., Jeffrey, P. D., Patten, A. K., Massagué, J., and Pavletich, N. P. (1996) Crystal structure of the p27Kip1 cyclin-dependent-kinase inhibitor bound to the cyclin A-Cdk2 complex. *Nature* **382**, 325–331 [CrossRef](#) [Medline](#)
50. Yamaguchi, F., Takata, M., Kamitori, K., Nonaka, M., Dong, Y., Sui, L., and Tokuda, M. (2008) Rare sugar D-allose induces specific up-regulation of TXNIP and subsequent G₁ cell cycle arrest in hepatocellular carcinoma cells by stabilization of p27kip1. *Int. J. Oncol.* **32**, 377–385 [CrossRef](#) [Medline](#)
51. Petri, E. T., Errico, A., Escobedo, L., Hunt, T., and Basavappa, R. (2007) The crystal structure of human cyclin B. *Cell Cycle* **6**, 1342–1349 [CrossRef](#) [Medline](#)
52. Pines, J., and Hunter, T. (1989) Isolation of a human cyclin cDNA: evidence for cyclin mRNA and protein regulation in the cell cycle and for interaction with p34cdc2. *Cell* **58**, 833–846 [CrossRef](#) [Medline](#)
53. Fang, G., Yu, H., and Kirschner, M. W. (1999) Control of mitotic transitions by the anaphase-promoting complex. *Philos. Trans. R. Soc. Lond. B Biol. Sci.* **354**, 1583–1590 [CrossRef](#) [Medline](#)
54. Nikonova, A. S., Astsaturov, I., Serebriiskii, I. G., Dunbrack, R. L., and Golemis, E. A. (2013) Aurora A kinase (AURKA) in normal and pathological cell division. *Cell Mol. Life Sci.* **70**, 661–687 [CrossRef](#) [Medline](#)
55. Jang, C. Y., Wong, J., Coppinger, J. A., Seki, A., Yates, J. R., and Fang, G. (2008) DDA3 recruits microtubule depolymerase Kif2a to spindle poles and controls spindle dynamics and mitotic chromosome movement. *J. Cell Biol.* **181**, 255–267 [CrossRef](#) [Medline](#)
56. Kabeche, L., Nguyen, H. D., Buisson, R., and Zou, L. (2018) A mitosis-specific and R loop-driven ATR pathway promotes faithful chromosome segregation. *Science* **359**, 108–114 [CrossRef](#) [Medline](#)
57. Ziv, Y., Bielopolski, D., Galanty, Y., Lukas, C., Taya, Y., Schultz, D. C., Lukas, J., Bekker-Jensen, S., Bartek, J., and Shiloh, Y. (2006) Chromatin relaxation in response to DNA double-strand breaks is modulated by a novel ATM- and KAP-1 dependent pathway. *Nat. Cell Biol.* **8**, 870–876 [CrossRef](#) [Medline](#)
58. Myers, J. S., and Cortez, D. (2006) Rapid activation of ATR by ionizing radiation requires ATM and Mre11. *J. Biol. Chem.* **281**, 9346–9350 [CrossRef](#) [Medline](#)
59. Yazinski, S. A., Comaills, V., Buisson, R., Genois, M. M., Nguyen, H. D., Ho, C. K., Todorova Kwan, T., Morris, R., Lauffer, S., Nussenzweig, A., Ramaswamy, S., Benes, C. H., Haber, D. A., Maheswaran, S., Birrer, M. J., et al. (2017) ATR inhibition disrupts rewired homologous recombination and fork protection pathways in PARP inhibitor-resistant BRCA-deficient cancer cells. *Genes Dev.* **31**, 318–332 [CrossRef](#) [Medline](#)
60. Karnitz, L. M., and Zou, L. (2015) Molecular pathways: targeting ATR in cancer therapy. *Clin. Cancer Res.* **21**, 4780–4785 [CrossRef](#) [Medline](#)
61. Flynn, R. L., Cox, K. E., Jeitany, M., Wakimoto, H., Bryll, A. R., Ganem, N. J., Bersani, F., Pineda, J. R., Suvà, M. L., Benes, C. H., Haber, D. A., Boussin, F. D., and Zou, L. (2015) Alternative lengthening of telomeres renders cancer cells hypersensitive to ATR inhibitors. *Science* **347**, 273–277 [CrossRef](#) [Medline](#)
62. Abiko, Y., Arai, J., Mitamura, J., and Kaku, T. (1997) Alteration of proto-oncogenes during apoptosis in the oral squamous cell carcinoma cell line, SAS, induced by staurosporine. *Cancer Lett.* **118**, 101–107 [CrossRef](#) [Medline](#)
63. Takahashi, A. (2001) Different inducibility of radiation- or heat-induced p53-dependent apoptosis after acute or chronic irradiation in human

- cultured squamous cell carcinoma cells. *Int. J. Radiat. Biol.* **77**, 215–224 [CrossRef](#) [Medline](#)
64. Kanata, H., Yane, K., Ota, I., Miyahara, H., Matsunaga, T., Takahashi, A., Ohnishi, K., Ohnishi, T., and Hosoi, H. (2000) CDDP induces p53-dependent apoptosis in tongue cancer cells. *Int. J. Oncol.* **17**, 513–517 [CrossRef](#) [Medline](#)
65. Sakai, E., and Tsuchida, N. (1992) Most human squamous cell carcinomas in the oral cavity contain mutated p53 tumor-suppressor genes. *Oncogene* **7**, 927–933 [Medline](#)
66. Schneider, C. A., Rasband, W. S., and Eliceiri, K. W. (2012) NIH Image to ImageJ: 25 years of image analysis. *Nat. Methods* **9**, 671–675 [CrossRef](#) [Medline](#)
67. Kim, D., Langmead, B., and Salzberg, S. L. (2015) HISAT: a fast spliced aligner with low memory requirements. *Nat. Methods* **12**, 357–360 [CrossRef](#) [Medline](#)
68. Pertea, M., Kim, D., Pertea, G. M., Leek, J. T., and Salzberg, S. L. (2016) Transcript-level expression analysis of RNA-seq experiments with HISAT, StringTie and Ballgown. *Nat. Protoc.* **11**, 1650–1667 [CrossRef](#) [Medline](#)
69. Pertea, M., Pertea, G. M., Antonescu, C. M., Chang, T. C., Mendell, J. T., and Salzberg, S. L. (2015) StringTie enables improved reconstruction of a transcriptome from RNA-seq reads. *Nat. Biotechnol.* **33**, 290–295 [CrossRef](#) [Medline](#)
70. Robinson, M. D., and Smyth, G. K. (2008) Small-sample estimation of negative binomial dispersion, with applications to SAGE data. *Biostatistics* **9**, 321–332 [CrossRef](#) [Medline](#)
71. Robinson, M. D., McCarthy, D. J., and Smyth, G. K. (2010) edgeR: a Bioconductor package for differential expression analysis of digital gene expression data. *Bioinformatics* **26**, 139–140 [CrossRef](#) [Medline](#)
72. Pomaznoy, M., Ha, B., and Peters, B. (2018) GOnet: a tool for interactive Gene Ontology analysis. *BMC Bioinformatics* **19**, 470 [CrossRef](#) [Medline](#)